https://dx.doi.org/10.1016/j.ijrmms.2020.104267

An Excess Stress Model for Capturing Rate-dependent Compressive Behavior of Rock Joint and Its Validation and Applications

Hua LI (Li H.)[1,2], Tao ZHOU (Zhou T.)[3], Jianhui DENG (Deng J. H.) [1], Jian-Hua YIN (Yin J.H.)[2], Jianbo ZHU (Zhu J.B.) [4*]

[1] State Key Laboratory of Hydraulics and Mountain River Engineering, Sichuan University, Chengdu, China

[2] Department of Civil and Environmental Engineering, The Hong Kong Polytechnic University, Hong Kong, China

[3] Guangdong Provincial Key Laboratory of Deep Earth Sciences and Geothermal Energy Exploitation and Utilization, Institute of Deep Earth Sciences and Green Energy, College of Civil and Transportation Engineering, Shenzhen University, Shenzhen, China

[4] State Key Laboratory of Hydraulic Engineering Simulation and Safety, School of Civil Engineering, Tianjin University, Tianjin, China

* Corresponding author, Email: jbzhu@tju.edu.cn
Webpage: http://jgxy.tju.edu.cn/teachers.asp?id=256

Abstract:

The deformational and mechanical behavior of rock masses is determined by discontinuities at different scales, e.g., rock joints. The discontinuous rock masses are often subjected to dynamic loads, e.g. blasts and earthquakes. Therefore, understanding dynamic response of rock joints is crucial. However, the dynamic compressive characteristics of rock joints have not been well understood yet. In this study, an excess stress model, employing the mechanical conceptual models based on the Hooke, the modified Saint Venant and the Newton elements, was developed. It is capable of capturing the nonlinear compressive processes of joints at different loading rates. This new model was validated by the comparison between model predictions and laboratory measurements obtained at loading rates ranging from approximately 200 GPa/s to 600 GPa/s. It was found that certain of rate-dependent compressive characteristics of rough joints can be successfully quantified with the proposed joint model. Compressive strength can be approximately predicted on the assumption that the peak-stress displacement is independent of the loading rate. Both the peak-stress secant stiffness and tangent stiffness predicted by the new joint model increase linearly with the loading rate. The wave energy dissipation at joints calculated by the proposed model decreases with increasing loading rate. Based on this model, the underlying mechanisms responsible for loading rate effects were related to the rate-dependency of crack propagation. Two hypotheses have been proposed: 1)the amount of cracking decreases with the increase of loading rate before the peak stress, causing ‘apparent’ hardening effects; 2) crack propagation velocity is relatively steady under static/quasi-static conditions, but becomes increasingly unstable when the loading rate is higher than the critical transition value. The present findings potentially provide a mechanically sound frame for the rate-dependent characteristics of joints, and have important implications for explicating the rate-dependent phenomena of fracturing, such as crack branching and fracture smoothening.

Keywords: Rock joint; Excess stress model; Dynamic compression; Rate dependency

List of symbols

σ_H	Stress in the Hooke model
u_H	Displacement in the Hooke model
k_1	Spring stiffness in the Hooke model
σ_{M_S}	Stress in the S_m model
u_{M_S}	Displacement in the S_m model
k_2	Spring stiffness in the S_m model
θ	Dip angle of frictional surfaces in the S_m model
φ	Fictional angle of frictional surfaces in the S_m model
σ_N	Stress in the Newton model
u_N	Displacement in the Newton model
η	Dynamic viscosity
t	Time
R	Loading rate
σ	Total stress of the H-S_m/N model
u	Total displacement of the H-S_m/N model
σ_p	Compressive strength of joints in one cycle of a pulse excitation
u_c	Displacement corresponding to the compressive strength
C	X-axis intercept of the unloading curve
u_j	Joint deformation
u_s	Total deformation of joint specimens
u_r	Deformation cause by intact rock
E_d	Dynamic Young's modulus of intact rock
l_s	Length of joint specimens
l_j	Joint thickness
σ_s	Static/reference compressive strength
σ_d	Dynamic compressive strength
k_d	Tangential compressive stiffness
ω	Maximum stored energy at joints
$\Delta\omega$	Dissipated energy at joints
E_S	Strain energy consumed in the joint specimen
$Q_{seismic}$	Seismic quality factor
β	Empirical parameter in the power-law expression of DIF
A, B, and m	Fitting constants in the H-S_m/N model
E_I, E_R, and E_T	Strain energy carried by incident, reflected and transmitted waves
ε_I, ε_R, and ε_T	Strain caused by incident, reflected and transmitted waves
A_B, C_B and E_B	Cross-section area, elastic wave velocity, and Young's modulus of bar material

1 Introduction

Discontinuous rock masses are often subjected to dynamic loads, e.g., blasts, impacts and earthquakes, where the strain rate would be higher than 10^{-2} s^{-1} and the rate-dependent behavior of joints becomes significant (Hencher, 1981; Zhao et al., 2006). To date, two general agreements on the rate dependency in joint compressive behavior have been reached. First, joint compressive strength and joint stiffness rise with the increase of strain rate (Li et al., 2017; Zhang & Zhao, 2014; Zhu et al., 2018b). Second, the compressive behavior of joints remains nonlinear under dynamic conditions (Barton et al., 1985; Ma et al., 2010; Wu et al., 2012). However, this rate dependency is still illy defined, as joint compression is dominated by multiple factors, e.g., joint/rock properties, contact conditions and loading process. This complexity requires more effective rate-dependent joint models and more refined testing techniques to satisfy the needs for quantitatively examining the rate-dependent behavior of joints, which is of great significance in the reliable design of rock structures.

Some static/quasi-static models have been developed to describe the nonlinear joint compressive behavior. A widely used empirical model is the Bandis-Barton model (Bandis et al., 1983; Barton et al., 1985), which is a typical hyperbolic function taking the form in line with the models proposed by Goodman (1976) and Kulhawy (1975). These models are usually regarded as stress-based models, which take no account of initial closure conditions and compressive failure conditions of asperities. In contrast, the logarithmic models (Brown & Scholz, 1986; Swan, 1981) are usually categorized as displacement-based models due to its sensitivity to initial contact and closure of joints (Zhao & Brown, 1992). Besides, exponential models (Jaeger et al., 2009) and power models (Cui et al., 2017; Cundall & Lemos, 1990) were also developed to describe the nonlinear compressive process of joints, which were originally proposed to simulate the joint nonlinearity during in situ tests. Unfortunately, these static/quasi-static joint models were not applicable to unloading phases, thus unable to reflect the whole compression processes of joints subjected to pulse/dynamic excitations.

Strong strain rate effects commonly exist for the dynamic behavior of brittle materials such as rock. Among the reasons for strain rate effects, two possible explanations are more discussed in the previous studies. Some studies, e.g., Sigenori et al. (1977); Zhao (1998); Zheng and Li (2004), reckoned that the strain rate effect is equivalent to the viscosity effect. It was suggested

that the tensile stress applied perpendicular to the plane of microcracks is in proportion to the opening velocity and the viscosity of the filled liquid (Barton, 1988; Zheng & Li, 2004). Thus, a higher loading/strain rate would induce a higher cohesive force between the crack surfaces. Another explanation correlates the strain rate effect to the inertia effect. At the micro scale, the inertia effect could be reckoned as the increased resistance at crack tips to any sudden changes in position and state of motion (Ragueneau & Gatuingt, 2003). This increment in force is usually expressed as a function of particle acceleration (Liao et al., 2016; Zhu et al., 2016), and contributes to the stiffness hardening/enhancement at the macro scale. In fact, the cracking mechanisms on joint surfaces and in adjacent rock blocks are likely to be different, due to the visible aperture between joint surfaces. Unlike the strain rate effect of rock material, the understanding of rate dependency of joint compressive behavior is still in its infancy.

Currently, most of the existing models for reproducing joint dynamic behavior were developed based on phenomenological assumptions, which are usually simple and direct. Usually, the static joint model was extended to dynamic conditions through introducing a rate-related correction factor (Johnson & Cook, 1985). For example, the Bandis-Barton model (Bandis et al., 1983; Barton et al., 1985) was extended to dynamic tests by taking the assumption that the rate-dependent effect could be entirely reflected by the change of material parameters i.e., initial stiffness and maximum allowable closure (Ma et al., 2010; Zhao & Cai, 2001). Another group of joint dynamic models were established based on the assumption on plastic/viscoplastic strain rate (Schneider, 1977; Sigenori et al., 1977). These models are usually called excess stress models, where the total strain rate is assumed to be the sum of elastic strain rate and viscoplastic/plastic strain rate (Perzyna, 1966), and thus, the total strain of joints becomes the sum of the static (rate-independent) component and the dynamic (rate-dependent) component (Zhu et al., 2018a). However, the link between these assumptions and the mechanisms of stain rate effects was rarely mentioned in the previous studies. Therefore, the reasonability of these assumptions and the accuracy of the model predictions were undetermined.

Moreover, it is widely accepted that constitutive relations and strength criteria determine the mechanical properties of materials, and wave energy attenuation is affected by the mechanical and physical properties of the bearing material (Pyrak-Nolte et al., 1996; Zhu et al., 2011). Therefore, it is desirable to study the wave energy dissipation at rock joints from the perspectives

of joint constitutive relations. Not only is it a reasonable approach to model validation, but it gives clues as to the accuracy of our laboratory testing results. The gap between energy dissipation and joint constitutive relation is bridged by joint mechanical parameters, e.g., strength and stiffness, which determine the compressive behavior of joints as well as the stress wave propagation at joints. Although extensive studies have been conducted to study the seismic response of joints (Li et al., 2012; Pyrak-Nolte, 1996; Zhao & Cai, 2001; Zhao et al., 2003), the rate dependency of wave energy dissipation at rock joints is still poorly understood.

The aim of this paper is to propose a dynamic model of rock joints to reflect the rate dependency of strength, stiffness and energy dissipation in the entire compression process of joints subjected to pulse excitations. First, an elastic-viscoplastic model was proposed employing the mechanical conceptual models based on dashpots and springs. It was validated by the comparison between testing results and model predictions. Rate dependency of joint strength, stiffness and energy dissipation in one cycle of a pulse excitation was then systematically studied, and the loading rate effect was elaborated from the perspective of crack propagation. The present findings help to understand the dynamic compression response of joints and potentially provide a mechanically sound frame for the study on the rate-dependent characteristics of joints.

2 The H-S_m/N model

The proposed dynamic model of joints is composed of the Hooke, the modified Saint Venant (S_m) (Zhu et al., 2018a) and the Newton elements, as shown in Fig.1. Here, Hooke element is introduced to reflect the elastic/recoverable deformation. Newton element is introduced to incorporate the additional time-related stress component under dynamic conditions. And the Saint Venant model is introduced and modified to reflect the irreversible hardening process. Since the rate-dependent effect of rock and rock-like materials could be explicated by the opening of microcracks, the Newton element is connected in parallel with the modified Saint Venant model to reflect the rete-dependent cracking process in compression. The stress-displacement relationship of the proposed model is derived below.

For the Hooke element:

$$\sigma_H = k_1 u_H = f(u_H) u_H = F(u_H) \quad (1)$$

where σ_H and u_H are stress and displacement, respectively; k_1 is the spring stiffness, which can be a constant or a function of displacement $f(u_H)$ representing linear or nonlinear elastic behavior, respectively. In this study, spring stiffness is taken positive under compressive/loading conditions.

For the S_m element:

$$\sigma_{M\_S} = 2k_2 \tan\theta \tan(\varphi+\theta) u_{M\_S} \quad (2)$$

where σ_{M_S} and u_{M_S} are stress and displacement, respectively; k_2 is the spring stiffness; θ and φ are the dip angle and fictional angle of frictional surfaces, respectively.

For the Newton element:

$$\sigma_N = \eta \frac{du_N}{dt} \quad (3)$$

$$\frac{d\sigma_N}{dt} = \eta \frac{d^2 u_N}{dt^2} \quad (4)$$

where σ_N, u_N are stress and displacement, respectively; t is time; η is the dynamic viscosity in $MPa \cdot S/mm$. η can be considered as a nearly invariable constant at the loading rate from 10^2 to 10^3 GPa/s and equals to 0.001 MPa·s/mm in the present study, according to Pyrak-Nolte (1988).

Since the Newton element is connected in parallel with the modified Saint Venant element, the total displacement u and stress σ of the H-S_m/N model satisfy the following equations:

$$u_N = u_{M\_S} \quad (5)$$

$$\sigma = \sigma_H = \sigma_{M\_S} + \sigma_N \quad (6)$$

$$u = u_H + u_N = u_H + u_{M\_S} \quad (7)$$

$$\frac{d\sigma}{dt} = \frac{d\sigma_H}{dt} = R \quad (8)$$

where R is the loading rate.

Therefore, the total stress of the H-S_m/N model can be expressed as:

$$\sigma = \sigma_H = k_1 u_H = \eta \frac{du_N}{dt} + 2k_2 \tan\theta \tan(\varphi + \theta) u_{M\_S} \quad (9)$$

Taking its derivative with respect to time *t*, we have:

$$\frac{d\sigma}{dt} = \frac{d\sigma_H}{dt} = k_1 \frac{du_H}{dt} = \eta \frac{d^2 u_{M\_S}}{dt^2} + 2k_2 \tan\theta \tan(\varphi + \theta) \frac{du_{M\_S}}{dt} = R \quad (10)$$

Thus, the deformation velocity of the S_m element is:

$$\frac{du_{M\_S}}{dt} = c_1 \exp\left(-\frac{2tk_2 \tan\theta \tan(\varphi + \theta)}{\eta}\right) + \frac{R}{2k_2 \tan\theta \tan(\varphi + \theta)} \quad (11)$$

If R is a constant, the displacement of the S_m element can be expressed as:

$$u_{M\_S} = \frac{Rt}{2k_2 \tan\theta \tan(\varphi + \theta)} - \frac{c_1 \eta \exp\left(-\frac{2tk_2 \tan\theta \tan(\varphi + \theta)}{\eta}\right)}{2k_2 \tan\theta \tan(\varphi + \theta)} + c_2 \quad (12)$$

Similarly, the displacement of the Hooke element can be rewritten as:

$$u_H = \frac{Rt}{k_1} + c_3 \quad (13)$$

When *t* equals to zero, i.e., at the beginning of loading process, u_H, u_{M_S} and du_{M_S}/dt all equal to zero. Thus, values of c_1, c_2 and c_3 are derived:

$$c_1 = -\frac{R}{2k_2 \tan\theta \tan(\varphi + \theta)} \quad (14)$$

$$c_2 = -\frac{R\eta}{\left[2k_2 \tan\theta \tan(\varphi + \theta)\right]^2} \quad (15)$$

$$c_3 = 0 \quad (16)$$

Bringing Eqs. (12)-(15) into Eq. (7), the expression of u as a function of σ is obtained:

$$u = \frac{\sigma}{k_1} + \frac{\sigma}{2k_2 \tan\theta \tan(\varphi + \theta)} + \frac{\eta R}{\left[2k_2 \tan\theta \tan(\varphi + \theta)\right]^2} \left[\exp\left(-\frac{2\sigma k_2 \tan\theta \tan(\varphi + \theta)}{\eta R}\right) - 1\right] \quad (17)$$

In the present study, physical meanings of θ and φ in joint compression have not been examined in depth. The two parameters were simply combined and defined as a displacement-related variable, reflecting the continuous yielding/hardening process:

$$\tan\theta\tan(\varphi+\theta)=\frac{u}{u_c} \qquad (18)$$

where u_c is the displacement corresponding to the peak stress.

Thus, Eq. (17) would be rewritten as:

$$u=\frac{\sigma}{k_1}+\frac{\sigma}{2k_2\dfrac{u}{u_c}}+\frac{\eta R}{\left(2k_2\dfrac{u}{u_c}\right)^2}\left[\exp(-\frac{2k_2\sigma u}{\eta R u_c})-1\right] \qquad (19)$$

Eq. (19) indicates that at the beginning of compression deformation, both u and σ equal to zero.

Since $0\le u\le u_c$ and $0<\exp(-\dfrac{2k_2\sigma u}{\eta R u_c})\le 1$, Eq. (19) is further simplified as:

$$u=\frac{\sigma}{k_1}+\frac{\sigma}{2k_2\dfrac{u}{u_c}}+\frac{\eta R}{\left(2k_2\dfrac{u}{u_c}\right)^2}\left(\frac{u_c^m-u^m}{u_c^m}-1\right) \qquad (20)$$

To derive the explicit expression of $\sigma(u)$, $\exp(-\dfrac{2k_2\sigma u}{\eta R u_c})$ is replaced by a dimensionless term $\dfrac{u_c^m-u^m}{u_c^m}$ in Eq. (19). They both range from 0 to 1 and decrease with the increase of u. Mathematically speaking, the difference between Eqs. (19) and (20) can be fairly offset by the pre-determined empirical constant *m*.

Thus Eq. (17) is finally simplified as:

$$u=\frac{\sigma}{k_1}+\frac{\sigma u_c}{2k_2 u}-\frac{\eta R}{4k_2^2}\xi \qquad (21\text{-}1)$$

or

$$\sigma = \frac{k_1 u\left(4k_2^2 u + \eta R\xi\right)}{2k_2(2k_2 u + u_c k_1)} \quad (21\text{-}2)$$

$$\xi = \left(\frac{u}{u_c}\right)^{m-2} \quad (21\text{-}3)$$

Eq. (21) is the final expression of the proposed model.

3 Validation of the H-S_m/N model

3.1 Dynamic compression test

The dynamic compression test was conducted on a split Hopkinson pressure bar (SHPB) apparatus (Fig, 2a), which contains incident and transmitted bars with circular cross section of 38 mm in diameter and 3 m and 1.8 m in length, respectively. The longitudinal wave velocity of the bar material is 5,201 m/s, and the Young's modulus is 211 GPa. In the present study, an air-powered loading system was used to launch the striker. A thin flat piece of copper was selected as the pulse shaper, which was 10 mm in diameter and 1 mm in thickness. The copper disc was stuck in the center and on the impact-end surface of the incident bar to shape the incident pulse into a nearly half-sine waveform. The incident, reflected and transmitted strain signals are measured by two groups of strain gauges glued on the incident and transmitted bars.

Three groups of granite joints with artificial grooves/notches were prepared before the test. Each joint specimen is composed of two well-contacted cylindrical halves with the same size of around 38 mm in diameter and 20 mm in height. Orthogonally arranged grooves with different depths, i.e., 2 mm, 4 mm and 8 mm, were cut on one contact surface of joints to consider the effect of joint thickness. The other surface remains flat and smooth to guarantee good contact between the two halves of the joint. The widths of these grooves are the same at about 6 mm. The groove central lines were arranged at the same positions on all joint surfaces to ensure the same joint matching condition, which was quantified by joint matching coefficient (*JMC*). The value of *JMC* for the grooved joints is approximately 0.38. Fig. 2 shows the grooves engraved on the granite cylinders, and the alignment of joint specimen and the SHPB system. In this study, all joint specimens were labeled on the basis of the depth of the grooves, for example, "2-mm

Joints", "4-mm Joints" and "8-mm Joints". A series of impact tests were successively conducted on each joint specimen with the launching air pressures of 16.5 kPa, 17.2 kPa and 18.0 kPa, which generated pulses with loading rates ranging from approximately 200 GPa/s to 600 GPa/s in our tests. The exact value of loading rate was determined by the slope of the pre-peak linear portion of the incident stress-time curve. The selected loading rates for each joint specimen were expected to be not higher than the critical-state loading rate, at which macrocracks generate or the sample breaks into large fragments. The critical-state loading rates for the grooved joints range from approximately 600 GPa/s to 800 GPa/s, which were pre-determined by trial and error. Two tests were conducted under the same loading condition to ensure the repeatability and reliability of the results. The aim of this testing procedure is to investigate the compressive behavior of the joints at different loading rates.

The average dynamic Young's modulus of the intact granite block is 59.76 GPa, which was measured by the dynamic compression test of three intact granite cylinders at the loading rates of 633 GPa/s, 744 GPa/s and 796 GPa/s, respectively. The stress-displacement curves obtained are shown in Fig. 3. It is indicated that when the loading rate is lower than 633 GPa/s, the deformation of the intact granite cylinder seems to be elastic. Thus, deformation caused by the granite joint itself in our tests can be directly estimated:

$$u_j = u_s - u_r = u_s - \frac{\sigma(l_s - l_j)}{E_d} \qquad (22)$$

where u_j is joint deformation; u_s is the total deformation of joint specimens; u_r is the deformation cause by intact rock; σ is the stress; E_d is the dynamic Young's modulus of intact rock; l_s is the length of joint specimens; l_j is joint thickness, which is equivalent to the depth of grooves.

Noteworthily, there are two underlying assumptions in Eq. (22). First, deformation of joint specimen is the sum deformation caused by the joint itself and the adjacent rock matrix. Second, irreversible deformation results from the deformation of the joint itself, which is considered as the major factor for energy dissipation. Undoubtedly, these two assumptions are in accordance with the H-S_m/N model, which has been detailed in Section 2. Fig. 4 illustrates the typical compressive stress-displacement curve of a joint calculated by Eq. (22).

3.2 Determination of model parameters

The application of the proposed joint model includes two steps. First, the model parameters are calibrated based on the compressive stress-displacement curve obtained at a relatively low loading rate, namely the reference loading rate. In the present study, it is 260 GPa/s for 2-mm joints, 214 GPa/s for 4-mm joints, and 277 GPa/s for 8-mm joints. Then, the dynamic compressive behavior of the joint at the other loading rates can be predicted by Eq. (21), based on the pre-determined model parameters and the given loading rates.

The stress-displacement/time curve of joints obtained by SHPB tests shows clear loading and unloading processes, as shown in Fig.4, which can be directly used to calibrate the model parameters. Here, u_c is determined directly by the position of peak stress σ_p; R is defined as the slope of the stress-time curve in the loading phase, representing the average changing rate of stress in the specimen. The recoverable deformation of the joint, i.e., u_H, is estimated by the x-axis projected length of the unloading curve. k_1 is thus determined by the equation below:

$$k_1 = \frac{\sigma_p}{u_H} \quad (23)$$

The peak strength σ_p thus becomes a function of k_2:

$$\sigma_p = \frac{k_1\left(4k_2^2 u_c + \eta R\right)}{2k_2(2k_2 + k_1)} \quad (24)$$

If k_1 is reckoned as a constant, the stress-displacement relationship defined by Eq. (21-1) could be easily expressed by an explicit function, i.e., Eq. (21-2). If k_1 is reckoned nonlinear, e.g., being a function of displacement, the explicit expression of σ would become rigmarole and confusing. Therefore, for simplification, k_1 is defined as a constant in the loading process, equaling to the slope of the straight line connecting peak stress and the x-axis intercept of the unloading curve, as shown in Fig.4. For the unloading process, a simple hyperbolic function is adopted to reflect the nonlinear deformation process:

$$u_H = \frac{\sigma}{A + \frac{\sigma}{B}} + C \quad (25)$$

where σ decreases from the peak strength to zero; C is the x-axis intercept of the unloading curve, as shown in Fig. 4; A and B are fitting coefficients, satisfying the requirement that when the peak strength is reached, Eq. (25) is equivalent to Eq. (23).

In summary, there are eight parameters in the proposed joint mode. R, m, u_c, k_1 and k_2 correlate with joint deformation behaviour in the loading phase, and A, B and C refer to the unloading phase. Only three empirical parameters exist in the proposed mode, i.e., m, A and B. m determines the curvature of the loading curve, and A and B defines the curvature of the unloading curve. These three parameters can be easily determined by best fitting.

3.3 Model validation

Based on these pre-determined parameters, dynamic compressive behavior of joints at different loading rates can be predicted. Fig. 5 shows typical compressive stress-displacement relations from laboratory tests and the proposed H-S_m/N model. The fitting curves (dash lines) were plotted to calibrate the model parameters. C, u_c, k_1 and $k_2$were measured or calculated directly from these stress-displacement curves, and the values of m, A and B were obtained through a trial and error process. The predicted curves, including loading and unloading phases, were calculated by Eqs. (21) and (25) based on the pre-determined values of model parameters and the given loading rates. Table 1 lists the values of parameters used in the proposed joint model.

It can be seen from Fig. 5 that the laboratory measurements agree well with model predictions. For joints with the same groove depth, both predicted and measured values of x-axis intercept of unloading curves decrease with increasing loading rate, while the compressive strength and stiffness increase with the rise of loading rate. At a given loading rate, joints with deeper grooves have lower compressive strength and larger peak-stress displacement, indicating that compressive stiffness decreases with the increase of joint thickness.

Hence, the applicability and accuracy of the proposed H-S_m/N model in predicting joint dynamic deformational behavior in compression are validated. Note that the compressive strength was approximately predicted on the assumption that u_c (i.e., the displacement corresponding to the peak stress) is independent of the loading rate for one and the same joint specimen. This assumption is in line with the finding from Wakabayashi et al. (1980) that the loading rate

appears to have no effect on the strain at the maximum stress in the uniaxial compressive test of concrete specimens.

4 **Application of the H-S_m/N model and analysis**

4.1 **Joint compressive strength**

The dynamic strength of joints determined from the SHPB tests is dependent on the input energy, the shape of incident waves, loading paths, and joint/rock properties, etc. The strength-related assumption adopted in the present study ignores this multi-factor feature and relates the peak stress to a fixed compressive displacement determined at a reference loading rate. In other words, the compressive strength of joints estimated by the proposed joint model varies as a function of loading rate as well as a pre-determined material constant.

This algorithmic simplification is similar with the analytical method adopted in the study on the dynamic increase factor (DIF), which is usually used to describe the strength enhancement as a function of loading rate. Mihashi and Wittmann (1980) proposed a classic expression of DIF based on the thermodynamic and stochastic theories, with which the relationship between compressive strength and loading rate is:

$$\frac{\sigma_d}{\sigma_s}=\left(\frac{\dot{\sigma}_d}{\dot{\sigma}_s}\right)^{1/(\beta+1)} \quad (26)$$

where σ_s denotes the static/reference compressive strength at a reference loading rate of $\dot{\sigma}_s$; σ_d denotes the dynamic compressive strength at the loading rate of $\dot{\sigma}_d$; β is an empirical parameter, representing the material compressive properties.

Fig. 6 shows the predicted peak stresses by Eq. (24) and Eq. (26) at loading rates from 100 GPa/s to 700 GPa/s as well as the laboratory measurements from the SHPB tests. β used in Eq. (26) maintains constant regardless the change of loading rate, equal to 0.55, 0.14 and 0.3 for the 2-mm, 4-mm, and 8-mm joints, respectively. These values were determined based on the testing results at loading rates of 214 GPa/s and 404 GPa/s for 2-mm joints, 260 GPa/s and 412 GPa/s for 4-mm joints, and 277 GPa/s and 424 GPa/s for 8-mm joints. The predicted results from Eq. (24) showed that the joint compressive strength increases linearly with increasing loading rate,

showing significant rate dependence. This is coincident with the testing results from Bischoff and Perry (1991), who found that within the same order of magnitude, the relationship between material strength and loading/strain rate can be expressed by a linear function. It can be seen that the joint compressive strengths predicted by Eqs. (24) and (26) show notable difference at high loading rates, e.g., 500~700 GPa/s. Also, it is expectable that this difference would be more significant with further increase of loading rate. However, for the loading rates ranging from 200 GPa/s to 600 GPa/s in the present study, the difference is less than 15% and within an acceptable range. In contrast, good agreement was found between the compressive strengths predicted by Eqs. (24) and (26) at relatively low loading rates, e.g., 100~300 GPa/s. It suggests that the proposed joint model would have greater capacity to predict the joint compressive strength, when the loading rate is lower than the reference loading rate. The present results lead to a tentative conclusion that the joint compressive strength can be approximately predicted by the proposed joint model when the loading rate ranges from one third to three times as high as the reference loading rate, provided that u_c is independent of the loading rate.

4.2 **Compressive stiffness**

By taking the partial derivative of Eq. (21-2) with respect to u, the transient/tangential compressive stiffness of joints is defined as follows:

$$k_d = \frac{\partial \sigma}{\partial u} = p + qR$$
$$p = \frac{4k_1k_2^2u^2 + 4k_1^2u_ck_2u}{(k_1u_c + 2k_2u)^2} \quad (27)$$
$$q = \frac{\left[2k_1k_2u(m-2) + k_1^2u_c(m-1)\right]\eta u_c^2(u/u_c)^m}{2k_2u^2(k_1u_c + 2k_2u)^2}$$

where k_d denotes transient/tangential compressive stiffness, which increases with the rise of loading rate R from the outset.

Fig. 7 shows the predicted compressive stress-displacement relations of 2-mm joints as a function of loading rate using the H-S_m/N model. The adopted loading rates range from 100 GPa/s to 700 GPa/s. It can be seen that joint transient stiffness rises with the increase of compressive displacement, showing obvious rate-dependent characteristics. Note that the peak-

stress secant stiffness, i.e., the ratio of peak stress to the corresponding displacement, linearly increases with the loading rate. It rises significantly from 164.5 MPa/mm to 1067 MPa/mm with the increase of loading rate changing from 100 GPa/s to 700 GPa/s. This linear relationship has been mathematically expressed by Eq. (24). Similar to the compressive strength, the peak-stress secant stiffness was also determined on the assumption that u_c is independent of the loading rate.

When the loading rate tends to be infinitesimal, the value of the viscosity-related component in Eq. (21-2) becomes negligible. The compressive stress-displacement relation defined by Eq. (21-2) becomes rate-independent, representing the static compressive behavior of the joint. In other words, the rate-dependent H-S_m/N model 'degrades' into the rate-independent H-S_m model, when the loading rate is low enough. It is difficult to define how small the value should be in a general sense, as it varies with joint and rock properties. For 2-mm joints used in our tests, this value should be less than 1 MPa/s, where the difference between the predicted rate-dependent and rate-independent compressive strengths is less than 10%. The static compressive stress-displacement curve of 2-mm joints predicted by Eq. (21-2) is also plotted in Fig. 7. It is clear that the predicted compressive strength, secant stiffness and tangent stiffness are all much lower than those under dynamic conditions. It is reasonable to expect that the H-S_m/N model has the capability to reproduce the static compressive behavior of joints, when the loading rate is set to be sufficiently low.

4.3 **Energy dissipation**

Energy dissipation during stress wave propagation across rock joints is dependent on the physical and mechanical properties of the joints. In the displacement discontinuity model (Pyrak-Nolte et al., 1990), the magnitude of the transmission coefficient for *P*-wave pulses is in direct proportion to joint stiffness. Energy dissipation herein is estimated qualitatively by the seismic quality factor $Q_{seismic}$, which is to evaluate the seismic quality of rock and defined as the ratio of maximum stored energy ω to the dissipated energy $\Delta\omega$ in one cycle of an pulse excitation (Aki & Richards, 1980):

$$\frac{2\pi}{Q_{seismic}} = \frac{\Delta\omega}{\omega} \quad (28)$$

However, the method for determining $Q_{seismic}$ from SHPB tests has not been well developed. Two approaches were usually used in the previous studies. In the first approach, $Q_{seismic}$ is estimated by the deformation energy of joints measured directly from the compressive force-displacement curve (Li et al., 2019). As shown in Fig. 8, the area of the hysteresis loop, i.e., the area between loading and unloading curves, refers to the energy dissipated in one cycle of a pulse excitation, i.e., $\Delta\omega$. And the whole area under the loading curve donates the maximum stored energy in the joint during the test, i.e., ω. Thus, the ratio of $\Delta\omega$ to ω can be conveniently calculated without considering the dimension issue. Second, $Q_{seismic}$ can be also estimated by the elastic strain energy carried by the incident, reflected and transmitted waves, where one-dimensional stress wave propagation should be satisfied. In the SHPB test, the contribution of strain energy in the incident and transmitted bars to the sample deformation could be calculated as (Chen & Song, 2010):

$$E_S = E_I - E_R - E_T = \frac{1}{2} A_B C_B E_B T(\varepsilon_I^2 - \varepsilon_R^2 - \varepsilon_T^2) \quad (29)$$

where E_S is strain energy consumed in the joint specimen; A_B is the cross-section area of bars; C_B is the elastic wave velocity of the bar material; E_B is the Young's modulus of the bar material; T is the loading duration; E and ε denotes strain energy and strain, respectively. The subscripts, I, R, and T represent the incident, reflected and transmitted pulse, respectively.

Thus, the ratio of $\Delta\omega$ to ω can be calculated:

$$\frac{\Delta\omega}{\omega} = \frac{E_S\left(residual\right)}{E_S\left(max\right)} \quad (30)$$

With the known strain energy-compressive displacement curves of joints during wave propagation, the ratio could be determined. Here, we take the assumption that irreversible deformation occurs mainly at the joint.

In our study, the explicit expression of compressive stress as a function of displacement has been derived, i.e., Eqs. (21-2) and (25). Therefore, $\Delta\omega$ and ω can be also estimated by taking the integral of compressive stress over displacement. Similarly, $\Delta\omega$ and ω could be calculated by the area in the hysteresis loop and the area under the loading curve, respectively. The ratio of $\Delta\omega$ to ω can thus be calculated as:

$$\frac{\Delta\omega}{\omega}=\frac{\oint\sigma du}{\int_0^{u_c}\sigma du} \quad (31)$$

Fig. 9 shows the value of $2\pi/Q_{seismic}$ calculated by the above three methods using the stress wave, the force-displacement curve and the proposed joint model. In a general sense, the energy dissipated from joint deformation decreases with increasing loading rate, indicating that high loading rates bring about low wave energy dissipation at joints. The results calculated by the proposed model show good agreement with those from the compressive force-displacement curves. In contrast, the results by using stress waves show obvious difference. It may be attributed to the ignorance of the energy dissipation in rock matrix, which brings about imprecise energy estimations when cracking occurs in both joint and adjacent rock block. However, the relative error of the results from stress waves and the proposed joint model is still acceptable in our study. The maximum is less than 20% from the 2-mm joint at the loading rate of 260 GPa/s.

5. Discussion

With the proposed H-S_m/N model, the relationship between joint compressive stiffness and loading rate was determined by Eqs. (24) and (27). However, confusion arises about how to explain this strength/stiffness enhancement from the perspective of physical mechanisms. In the present study, two hypotheses were put forward based on the proposed H-S_m/N model and listed as follows.

Hypothesis 1. It can be seen from Fig. 5 that the x-axis intercept of unloading curves decreases with increasing loading rate, indicating that the irreversible deformation on joints deceases with the increase of loading rate. Thus, a hypothesis was proposed to explain this rate dependent hardening phenomenon: before the peak stress is reached, the amount of cracking decreases with increasing loading rate, causing ‘apparent’ hardening effects.

Hypothesis 2. The proposed joint model is a typical excess stress model, thus the stress increment in this model can be divided into rate-independent and rate-dependent components. Specifically, when the strain rate of the Newton element maintains constant, the stress increment of the H-S_m/N model only comes from the Hooke and modified Saint Venant elements. Joint

compressive stiffness at this time would be unaffected by the total strain rate, i.e., it is rate independent. In contrast, when the strain rate of the Newton element becomes alterable, the total stress increment would be affected by the Newton element. The compressive stiffness becomes a function of strain rate, showing rate dependence. Therefore, in the H-S_m/N model, this stiffness enhancement at high loading rates correlates with the strain rate of the Newton element, which represents irrecoverable deformation at the joint. Another hypothesis was thus proposed: crack propagation velocity is relatively steady under static/quasi-static conditions, but becomes increasingly unstable with the rise of loading rate, due to the change of fracturing patterns.

Although these hypotheses have not been justified in the present study, it is encouraging that they both follow what was indicated in the previous studies of dynamic crack propagation. As for Hypothesis 1, the concept of the decreasing amount of microcracks is in accordance with the interpretation of the strain/loading rate effect from Young and Powell (1979), who conducted a series of dynamic compression test of cylindrical rock specimens, and found that cracking starts from the free surface and propagates inwardly to the center of the specimens. With the rise of loading rate, time available for cracking is reduced, contributing to less deep-seated damage and greater load-carrying capacity (Young & Powell, 1979).

As for Hypothesis 2, the instability of crack propagation velocity is coincident with the existing explanations on the lateral inertial effect, which first becomes a consideration when the loading rate increases to $10^1 \sim 10^2$ GPa/s (Huang et al., 2010; Zhang & Zhao, 2013; Zhang & Zhao, 2014). With the increase of loading rates, time available for radial dilation (i.e., radial unloading to meet static equilibrium) is reduced, causing ‘extra’ confinement on the central core of the specimen (Janach, 1976). The presence of the confinement prevents the nucleation and growth of microcracks. Energy dissipation for cracking is thus restricted, leading to the increase of crack initiation toughness. When stress intensity factor increases to the critical value, energy dissipation for cracking probably becomes a sudden and unstable process. Crack-propagation velocity is more likely to exceed the limiting cracking velocity, which defines the velocity threshold for crack branching. Thus, more than one cracks would be activated simultaneously (Gillette et al., 1983; Soga et al., 1979), and brittle trans-granular fracturing occurs in order to release more energy (Atkinson, 1982; Cadoni et al., 2000). Fig. 10 shows typical joint failure patterns at loading rates of approximately 600 GPa/s and 800 GPa/s at both micro and macro

scales. The comparison between them provides straight evidence for the complex cracking/fracturing process. At the micro scale, more cracks were activated at higher loading rates. Most of them penetrated the grain boundary in the polycrystalline materials and continued to propagate along the original direction. As a result, a large number of fragments were generated. In contrast, joint specimens still retained their original shapes at the relatively low loading rate. Some micro-cracks appeared and kinked out to propagate along the boundary of grains or along the interface of different materials, leaving most of the polycrystalline material intact.

Although the SHPB tests were only conducted systematically at loading rates ranging from 200 GPa/s to 600 GPa/s in the present study, the agreement between the laboratory measurements and model predictions has proved the validity of the proposed joint model. Besides, simplifications were made in the derivation of the H-S_m/N model, i.e., Eqs (17) ~ (20). Although these simplifications were not proved by rigorous mathematical reasoning, the derived equations do not violate the original physical background of the H-S_m/N model.

The present findings help to understand the dynamic compressive behavior of joints. The proposed H-S_m/N model is reliable to evaluate the rate dependency of strength, stiffness and energy dissipation of joints in compression. It potentially provides a mechanically sound frame for the study on the rate-dependent characteristics of joints. The inferences about crack propagation give reasonable explanations of the loading rate effect. It has important implications for explicating the rate-dependent phenomena of fracturing, e.g., crack branching (Schardin & Struth, 1938) and fracture smoothening (Ramulu & Kobayashi, 1985), etc.

6 Conclusions

Main work and conclusions of this study are as follows:

1) An excess stress model was developed, employing the mechanical conceptual models based on the Hooke, the modified Saint Venant and the Newton elements, to describe the rate-dependent compressive behavior of rough joints. It is capable of reflecting the nonlinear hardening processes of joints at different loading rates. The proposed joint model was validated by the comparison between laboratory testing results and model predictions.

2) The compressive strength of joints can be approximately predicted by the proposed joint model within the range of loading rates from one third to three times as high as the reference loading rate, provided that u_c is independent of the loading rate. The predicted compressive strength of joint increases linearly with increasing loading rate, showing significant rate dependence.

3) The predicted compressive stress-displacement relation of joints shows apparent loading rate effects. Both the peak-stress secant stiffness and tangent stiffness increase linearly with the loading rate.

4) Wave energy dissipation at joints decreases with increasing loading rate. The wave energy dissipation calculated by the proposed model shows good agreement with that from the compressive stress-displacement curves but shows obvious difference from that by using stress wave.

5) Based on the developed joint model, the mechanism of loading rate effects is related to the rate-dependency of crack propagation. Two hypotheses were proposed: the amount of cracking decreases with the increase of loading rate before the peak stress, causing 'apparent' hardening effects; and crack propagation velocity becomes increasingly unstable with the rise of loading rate, due to the change of fracturing patterns.

Acknowledgements

This research is financially supported by the Hong Kong Jockey Club.

References

Aki, K., & Richards, P. (1980). *Quantitative seismology: Theory and methods*. Paper presented at the W. H. Freeman and Company, Newyork.

Atkinson, B. K. (1982). Subcritical crack propagation in rocks: theory, experimental results and applications. *Journal of Structural Geology, 4*(1), 41-56.

Bandis, S. C., Lumsden, A. C., & Barton, N. R. (1983). Fundamentals of rock joint deformation. *International Journal of Rock Mechanics and Mining Sciences & Geomechanics Abstracts, 20*(6), 249-268.

Barton, N. (1988). *Some aspects of rock joint behaviour under dynamic conditions*. Paper presented at the Mechanics and Engineering of Rocks Torino, Italy.

Barton, N., Bandis, S., & Bakhtar, K. (1985). Strength, deformation and conductivity coupling of rock joints. *International Journal of Rock Mechanics and Mining Sciences & Geomechanics Abstracts, 22*(3), 121-140.

Bischoff, P. H., & Perry, S. H. (1991). Compressive behaviour of concrete at high strain rates. *Materials and Structures, 24*(6), 425-450.

Brown, S. R., & Scholz, C. H. (1986). Closure of rock joints. *Journal of Geophysical Research: Solid Earth, 91*(B5), 4939-4948.

Cadoni, E., Labibes, K., Berra, M., Giangrasso, M., & Albertini, C. (2000). High-strain-rate tensile behaviour of concrete. *Magazine of Concrete Research, 52*(5), 365-370.

Chen, W. W., & Song, B. (2010). *Split Hopkinson (Kolsky) bar: design, testing and applications*: Springer Science & Business Media.

Cui, Z., Sheng, Q., Leng, X., & Ma, Y. (2017). Analysis of the Seismic Performance of a Rock Joint with a Modified Continuously Yielding Model. *Rock Mechanics and Rock Engineering, 50*(10), 2695-2707.

Cundall, P. A., & Lemos, J. V. (1990). Numerical simulation of fault instabilities with a continuously-yielding joint model. *Rockbursts and Seismicity in Mines*, 147-152.

Gillette, D. R., Sture, S., Ko, H.-Y., Gould, M. C., & Scott, G. A. (1983). *Dynamic behavior of rock joints*. Paper presented at the The 24th U.S. Symposium on Rock Mechanics (USRMS), College Station, Texas.

Goodman, R. E. (1976). *Methods of geological engineering in discontinuous rocks* (1st ed.). New York, USA: West Publishing

Hencher, S. (1981). Friction parameters for the design of rock slopes to withstand earthquake loading *Dams and Earthquake* (pp. 74-89): Thomas Telford Publishing.

Huang, S., Xia, K., Yan, F., & Feng, X. (2010). An Experimental Study of the Rate Dependence of Tensile Strength Softening of Longyou Sandstone. *Rock Mechanics and Rock Engineering, 43*(6), 677-683.

Jaeger, J. C., Cook, N. G., & Zimmerman, R. (2009). *Fundamentals of rock mechanics* (Fourth ed.). Malden MA: Blackwell Publishing.

Janach, W. (1976). *The role of bulking in brittle failure of rocks under rapid compression.* Paper presented at the International Journal of Rock Mechanics and Mining Sciences & Geomechanics Abstracts.

Johnson, G. R., & Cook, W. H. (1985). Fracture characteristics of three metals subjected to various strains, strain rates, temperatures and pressures. *Engineering Fracture Mechanics, 21*(1), 31-48.

Kulhawy, F. H. (1975). Stress deformation properties of rock and rock discontinuities. *Engineering Geology, 9*(4), 327-350.

Li, J. C., Li, H. B., Ma, G. W., & Zhao, J. (2012). A time-domain recursive method to analyse transient wave propagation across rock joints. *Geophysical Journal International, 188*(2), 631-644.

Li, J. C., Li, N. N., Li, H. B., & Zhao, J. (2017). An SHPB test study on wave propagation across rock masses with different contact area ratios of joint. *International Journal of Impact Engineering, 105*, 109-116.

Li, J. C., Rong, L. F., Li, H. B., & Hong, S. N. (2019). An SHPB Test Study on Stress Wave Energy Attenuation in Jointed Rock Masses. *Rock Mechanics and Rock Engineering, 52*(2), 403-420.

Liao, Z. Y., Zhu, J. B., Xia, K. W., & Tang, C. A. (2016). Determination of Dynamic Compressive and Tensile Behavior of Rocks from Numerical Tests of Split Hopkinson Pressure and Tension Bars. *Rock Mechanics and Rock Engineering, 49*(10), 3917-3934.

Ma, G. W., Li, J. C., & Zhao, J. (2010). Three-phase medium model for filled rock joint and interaction with stress waves. *International Journal for Numerical and Analytical Methods in Geomechanics, 35*(1), 97-110.

Mihashi, H., & Wittmann, F. H. (1980). Stochastic approach to study the influence of rate of loading on strength of concrete. *HERON, 25 (3), 1980*.
Perzyna, P. (1966). Fundamental problems in viscoplasticity. *Advances in Applied Mechanics, 9*, 243-377.
Pyrak-Nolte, L. J. (1988). *Seismic visibility of fractures.* (Ph.D), Berkeley, University of California, United States.
Pyrak-Nolte, L. J. (1996). The seismic response of fractures and the interrelations among fracture properties. *International Journal of Rock Mechanics and Mining Sciences & Geomechanics Abstracts, 33*(8), 787-802.
Pyrak-Nolte, L. J., Myer, L. R., & Cook, N. G. W. (1990). Transmission of seismic waves across single natural fractures. *Journal of Geophysical Research: Solid Earth, 95*(B6), 8617-8638.
Pyrak-Nolte, L. J., Roy, S., & Mullenbach, B. L. (1996). Interface waves propagated along a fracture. *Journal of Applied Geophysics, 35*(2), 79-87.
Ragueneau, F., & Gatuingt, F. (2003). Inelastic behavior modelling of concrete in low and high strain rate dynamics. *Computers & Structures, 81*(12), 1287-1299.
Ramulu, M., & Kobayashi, A. S. (1985). Mechanics of crack curving and branching — a dynamic fracture analysis. In M. L. Williams & W. G. Knauss (Eds.), *Dynamic fracture* (pp. 61-75). Dordrecht: Springer Netherlands.
Schardin, H., & Struth, W. (1938). High‐Frequency Cinematographic Investigation of Breaking Process in Glass. *Glastechnische. Berichte., 16*(7), 219-227.
Schneider, H. (1977). The time dependence of friction of rock joints. *Bulletin of the International Association of Engineering Geology, 16*(1), 235-239.
Sigenori, K., Azuhiko, S., & Minoru, K. (1977). On the mechanical behaviour of rocks under impulsive loading. *Bulletin of the Faculty of engineering Hokkaido University, 83*, 51-62.
Soga, N., Spetzler, H., & Mizutani, H. (1979). *Comparison of single crack propagation in lunar analogue glass and the failure strength of rocks.* Paper presented at the Lunar and Planetary Science Conference Proceedings.
Swan, G. (1981). *Tribology And The Characterisation Of Rock Joints*. Paper presented at the The 22nd U.S. Symposium on Rock Mechanics Cambridge, Massachusetts.
Wakabayashi, M., Nakamura, T., Yoshida, N., Iwai, S., & Watanabe, Y. (1980). *Dynamic loading effects on the structural performance of concrete and steel materials and beams.* Paper presented at the Proc., 7th World Conf. on Earthquake Engineering.
Wu, W., Li, J. C., & Zhao, J. (2012). Loading Rate Dependency of Dynamic Responses of Rock Joints at Low Loading Rate. *Rock Mechanics and Rock Engineering, 45*(3), 421-426.
Young, C., & Powell, C. (1979). *Lateral inertia effects on rock failure in split-Hopkinson-bar experiments.* Paper presented at the 20th US Symposium on Rock Mechanics (USRMS).
Zhang, Q. B., & Zhao, J. (2013). Determination of mechanical properties and full-field strain measurements of rock material under dynamic loads. *International Journal of Rock Mechanics and Mining Sciences, 60*, 423-439.
Zhang, Q. B., & Zhao, J. (2014). A review of dynamic experimental techniques and mechanical behaviour of rock materials. *Rock Mechanics and Rock Engineering, 47*(4), 1411-1478.
Zhao, J. (1998). Rock mass hydraulic conductivity of the Bukit Timah granite, Singapore. *Engineering Geology, 50*(1), 211-216.
Zhao, J., & Brown, E. T. (1992). *Logarithmic relation for joint normal deformation under effective stress*. Paper presented at the ISRM Symposium: Eurock'92, Chester.
Zhao, J., & Cai, J. G. (2001). Transmission of elastic P-waves across single fractures with a nonlinear normal deformational behavior. *Rock Mechanics and Rock Engineering, 34*(1), 3-22.
Zhao, J., Cai, J. G., Zhao, X. B., & Li, H. B. (2006). Experimental study of ultrasonic wave attenuation across parallel fractures. *Geomechanics and Geoengineering, 1*(2), 87-103.

Zhao, J., Cai, J. G., Zhao, X. B., & Song, H. W. (2003). Transmission of elastic p-waves across single fracture with nonlinear normal deformation behavior. *Chinese Journal of Rock Mechanics and Engineering, 22*(1), 9-17.

Zheng, D., & Li, Q. (2004). An explanation for rate effect of concrete strength based on fracture toughness including free water viscosity. *Engineering Fracture Mechanics, 71*(16), 2319-2327.

Zhu, J. B., Li, H., & Deng, J. H. (2018a). A one-dimensional elastoplastic model for capturing the nonlinear shear behaviour of joints with triangular asperities based on direct shear tests. *Rock Mechanics and Rock Engineering*.

Zhu, J. B., Liao, Z. Y., & Tang, C. A. (2016). Numerical SHPB tests of rocks under combined static and dynamic loading conditions with application to dynamic behavior of rocks under in situ stresses. *Rock Mechanics and Rock Engineering, 49*(10), 3935-3946.

Zhu, J. B., Perino, A., Zhao, G. F., Barla, G., Li, J. C., Ma, G. W., & Zhao, J. (2011). Seismic response of a single and a set of filled joints of viscoelastic deformational behaviour. *Geophysical Journal International, 186*(3), 1315-1330.

Zhu, J. B., Zhou, T., Liao, Z. Y., Sun, L., Li, X. B., & Chen, R. (2018b). Replication of internal defects and investigation of mechanical and fracture behaviour of rock using 3D printing and 3D numerical methods in combination with X-ray computerized tomography. *International Journal of Rock Mechanics and Mining Sciences, 106*, 198-212.

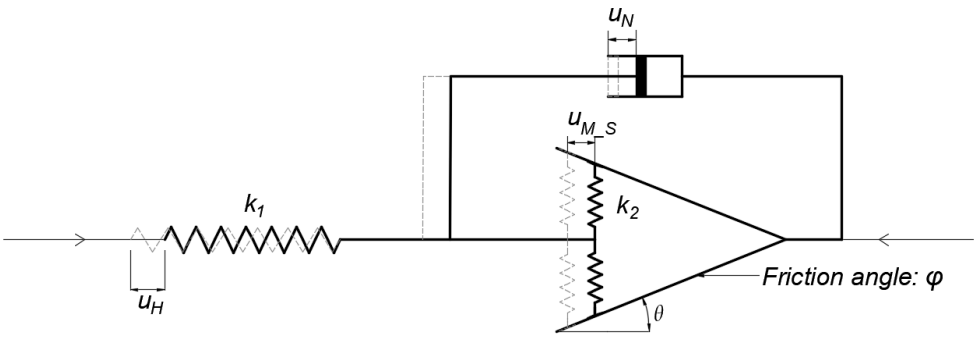

Fig. 1 Sketches of the Hooke-modified Saint Venant/Newton model. k_1 and k_2 are the spring stiffness; u_H, u_{M_S} and u_N represent the displacement of the Hooke, modified Saint Venant and Newton elements, respectively; θ and φ are the dip angle and fictional angle of frictional surfaces in the modified Saint Venant element, respectively.

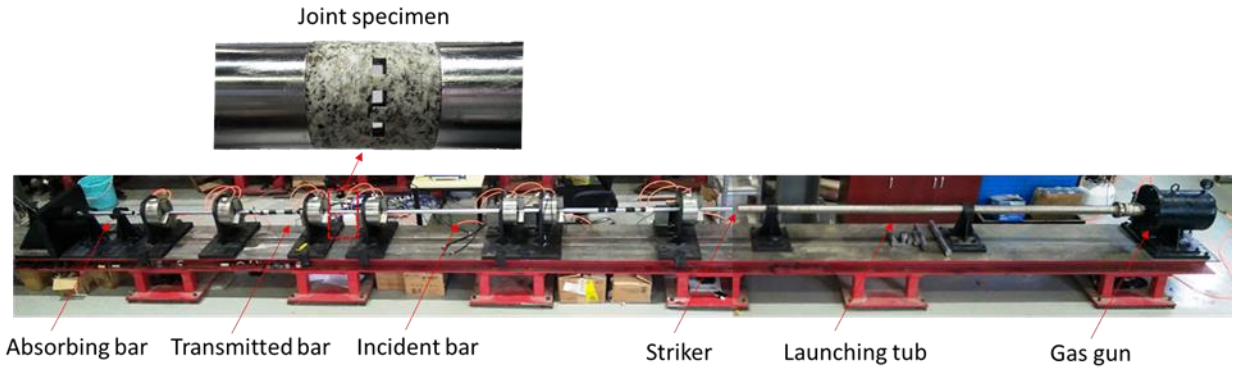

(a)

2 mm 4 mm 8 mm

(b)

Fig. 2 Joint specimens used in the SHPB test: (a) The SHPB system and the installation of joint specimen; (b) grooves engraved on the surface of the granite cylinders with different depths.

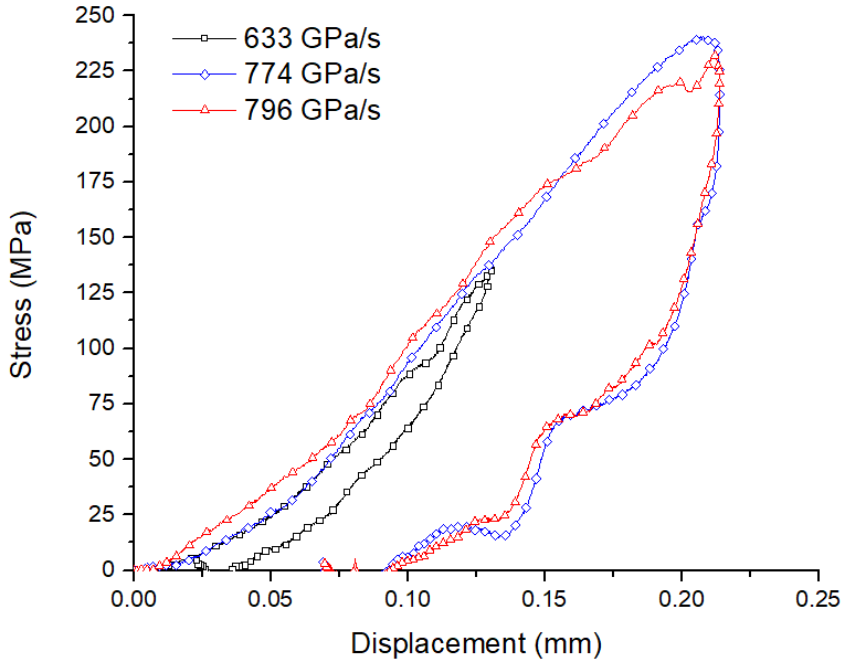

Fig. 3 The compressive stress-displacement curves of intact granite cylinders at different loading rates.

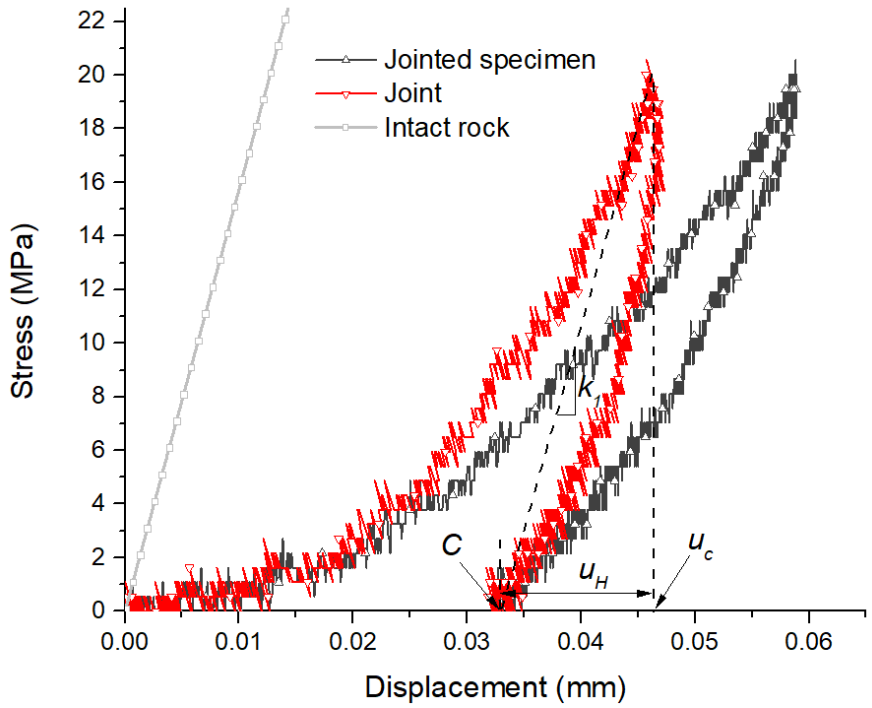

Fig. 4 A typical compressive stress-displacement curve of a joint calculated by Eq. (22). The deformation of jointed specimen is the sum deformation caused by the joint itself and the adjacent rock blocks. u_H represents the recoverable deformation of the joint; u_c is the compressive displacement at the peak-strength point; k_1 is the elastic/recoverable-deformation stiffness. Data come from the compression test of the joint with 2-mm grooves at the loading rate of 260 GPa/s.

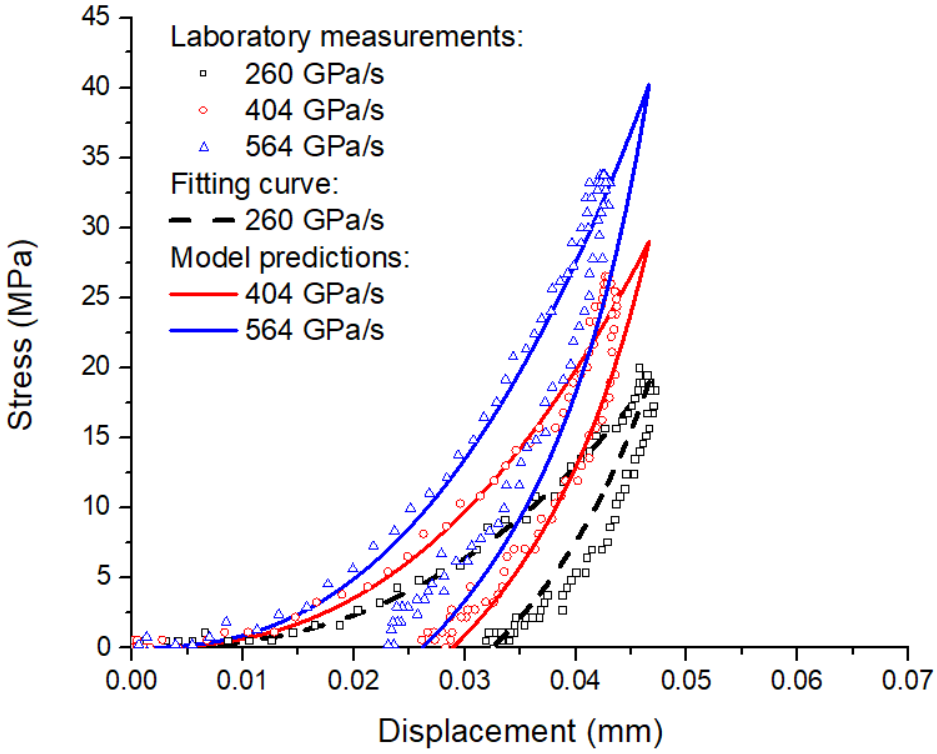
Laboratory measurements:
260 GPa/s
404 GPa/s
564 GPa/s
Fitting curve:
260 GPa/s
Model predictions:
404 GPa/s
564 GPa/s
Stress (MPa)
Displacement (mm)
0
5
10
15
20
25
30
35
40
45
0.00
0.01
0.02
0.03
0.04
0.05
0.06
0.07

(a)

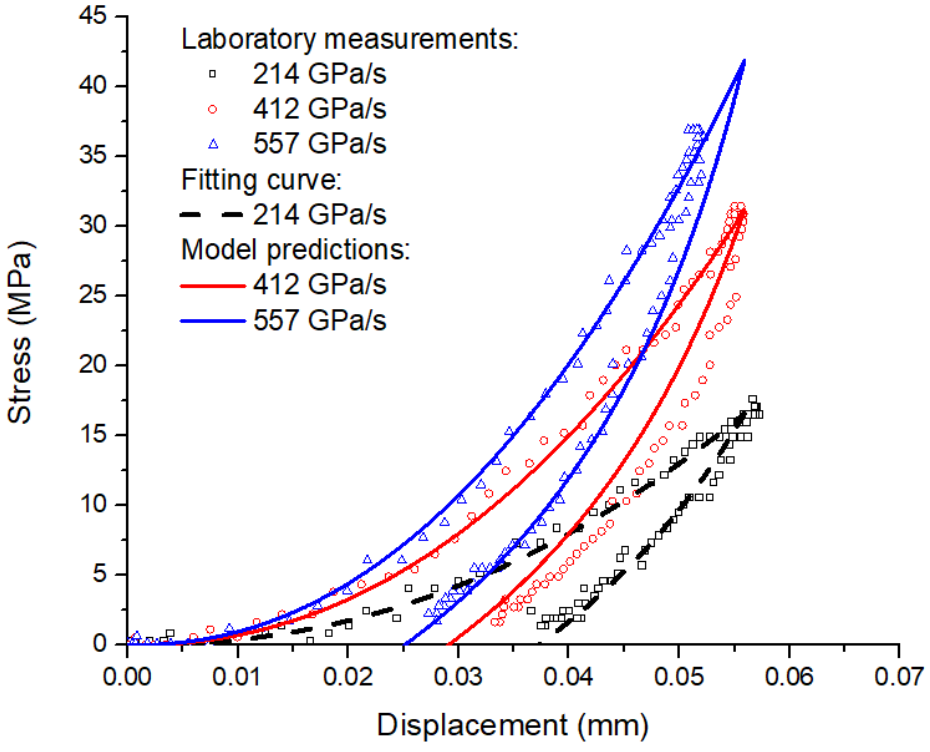
Laboratory measurements:
214 GPa/s
412 GPa/s
557 GPa/s
Fitting curve:
214 GPa/s
Model predictions:
412 GPa/s
557 GPa/s
Stress (MPa)
Displacement (mm)
0
5
10
15
20
25
30
35
40
45
0.00
0.01
0.02
0.03
0.04
0.05
0.06
0.07

(b)

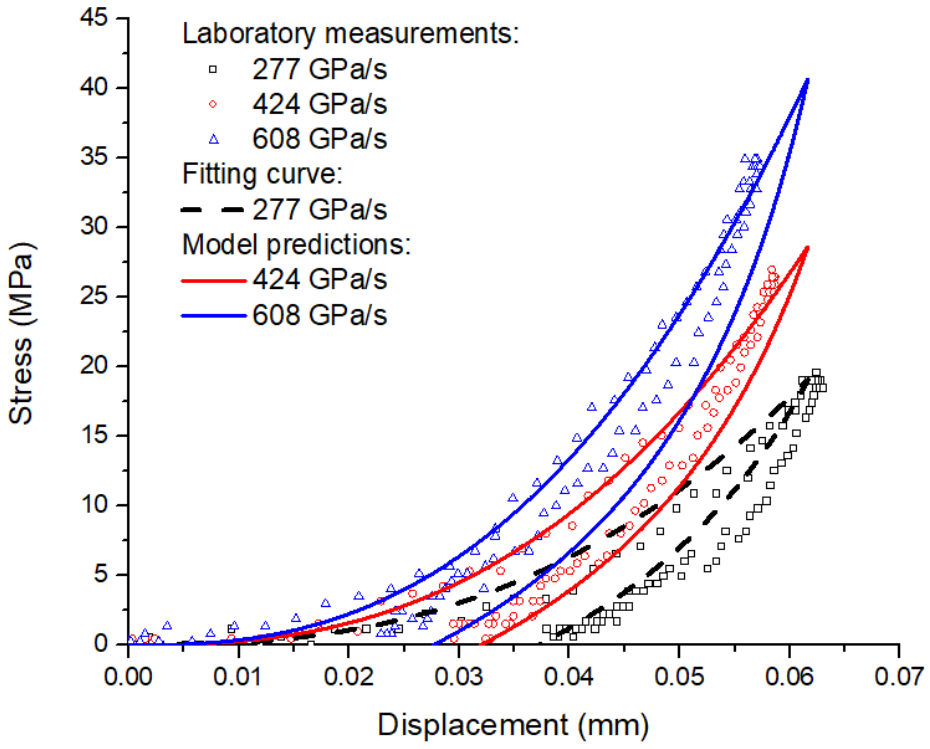

(c)

Fig.5 Compressive stress-displacement curves of joints with: (a) 2-mm; (b) 4-mm; and (c) 8-mm grooves from laboratory tests and the proposed H-S_m/N joint model at different loading rates. The fitting curves were used to calibrate model parameters.

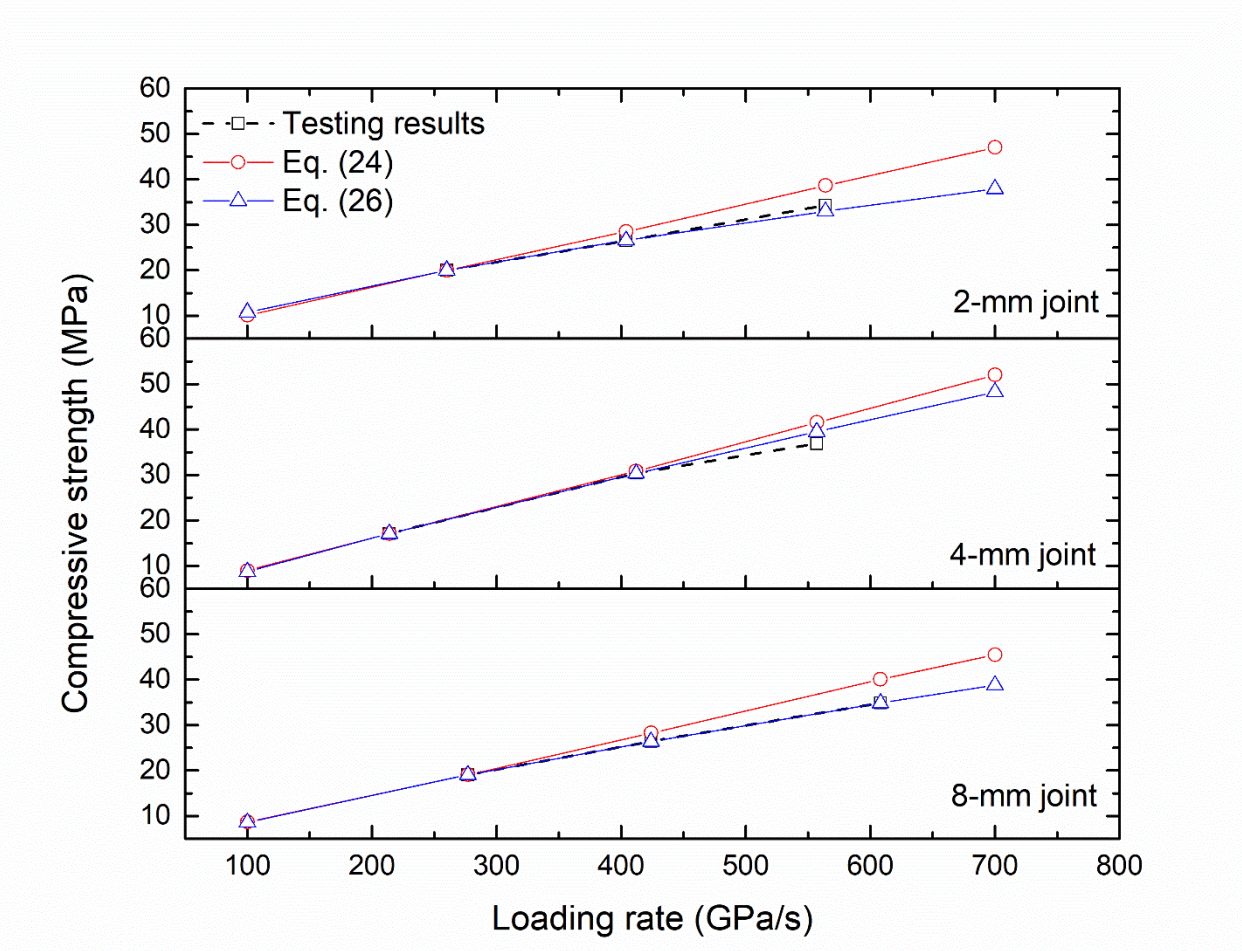

Fig. 6 The predicted joint compressive strength by Eq. (24) and Eq. (26) as well as laboratory measurements. β used in Eq. (26) maintains constant regardless the change of loading rate, equal to 0.55, 0.14 and 0.3 for the 2-mm, 4-mm, and 8-mm joints, respectively.

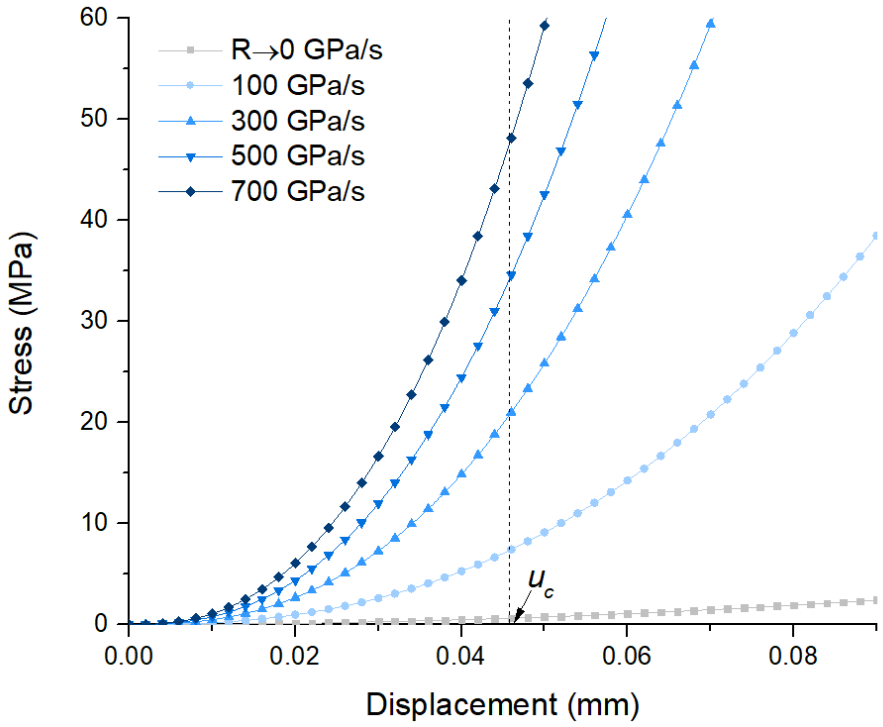

Fig. 7 The predicted compressive stress-displacement curves of 2-mm joints as a function of loading rate using the H-S_m/N model. u_c is the predicted compressive displacement at the peak strength determined by the laboratory test at the loading rate of 260 GPa/s.

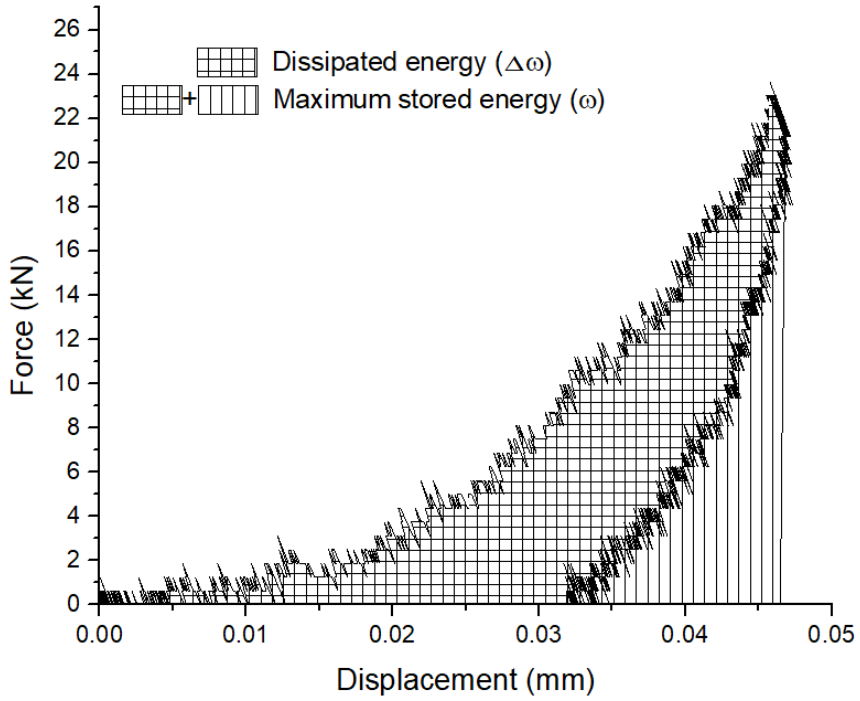

Fig. 8 The schematic view of $\Delta\omega$ and ω represented by the projected areas of the compressive force-displacement curve of joints. Data come from the compression test of the joint with 2-mm grooves at the loading rate of 260 GPa/s.

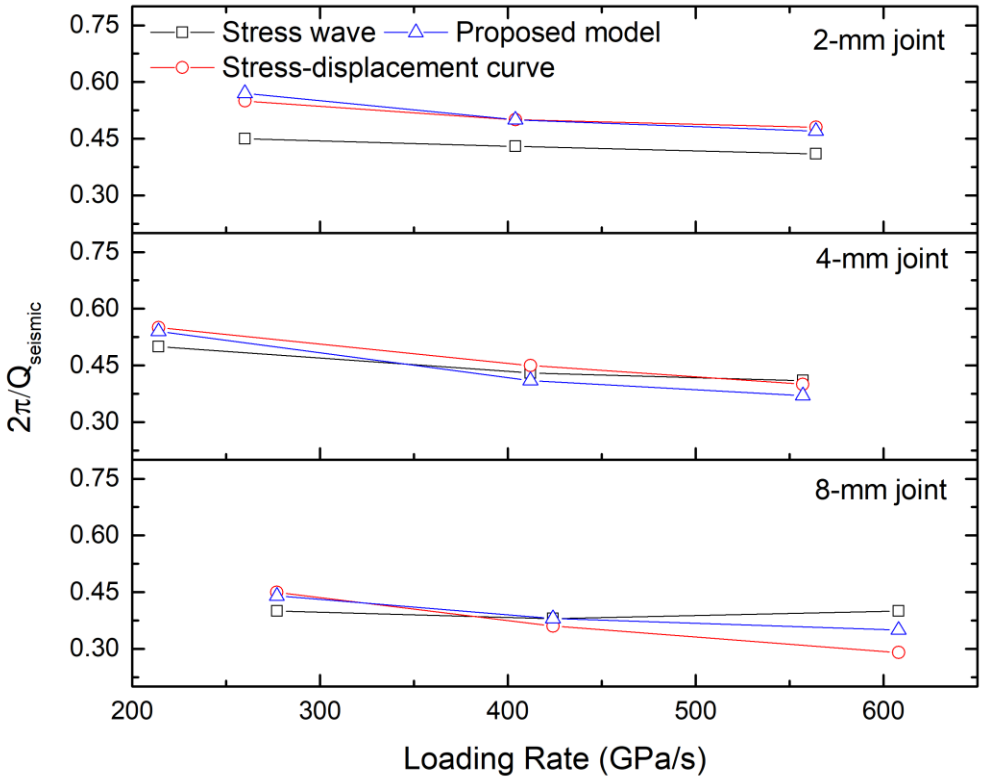

Fig. 9 $2\pi/Q_{seismic}$ calculated by using stress wave, force-displacement curve and the proposed joint model vs loading rate for 2-mm, 4-mm and 8-mm joints.

$\approx 600\ GPa/s$

$\approx 800\ GPa/s$

(a)

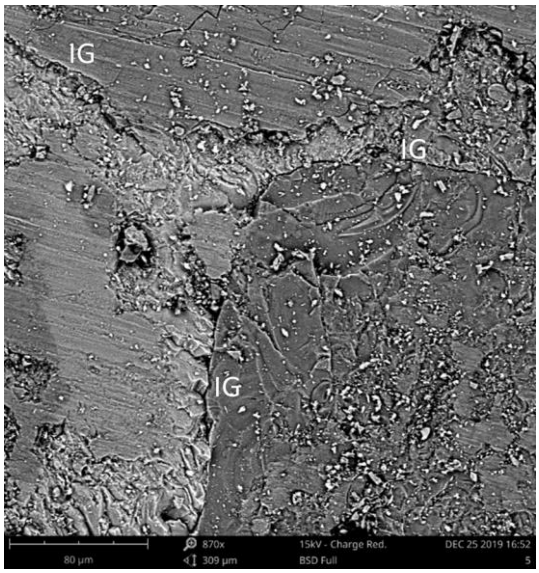

$\approx 600\ GPa/s$

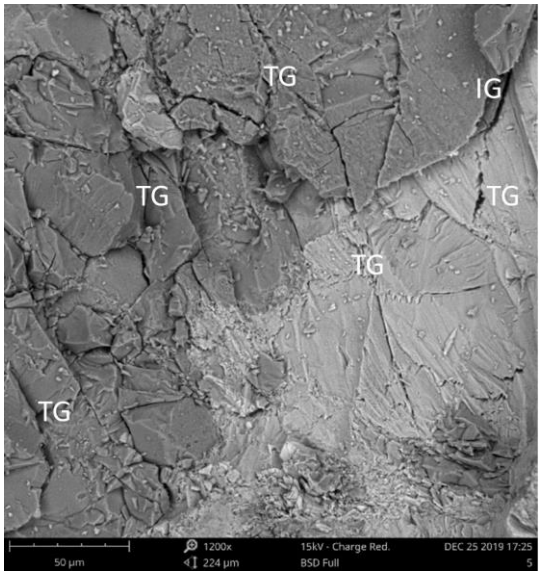

$\approx 800\ GPa/s$

(b)

Fig. 10 Typical failure patterns of 4-mm joints at loading rates of approximately 600 GPa/s and 800 GPa/s at macro and micro scales: (a) Fragments of damaged and failed joint specimens; (b) typical SEM micrographs of fractured joint asperities (IG: inter-granular fractures; TG: trans-granular fractures)

Table 1 The values of parameters used in the proposed joint model

Joint specimen	Model parameters						
	k_1 MPa/mm	k_2 MPa/mm	u_c mm	C mm	m --	A MPa/mm	B mm
2-mm Joint	1604.7627	7.0672	0.0466	0.0348	3.5	780	0.0338
4-mm Joint	941.717	6.6801	0.0559	0.0383	3.2	580	0.0538
8-mm Joint	826.6132	7.5126	0.0616	0.0386	3.6	410	0.0518